Solar Energy Materials & Solar Cells 295 (2026) 113989

Contents lists available at ScienceDirect

Solar Energy Materials and Solar Cells

journal homepage: www.elsevier.com/locate/solmat

Recombination activity of chromium-gallium pairs in silicon

Sanjida Sabah [a], Tien T. Le [a], Zhuangyi Zhou [b], Chang Sun [c], Yichun Wang [c], Nannan Fu [c], Fiacre Rougieux [b], Daniel Macdonald [a], AnYao Liu [a,*]

[a] School of Engineering, The Australian National University, Canberra, ACT, 2601, Australia
[b] School of Photovoltaic and Renewable Energy Engineering, University of New South Wales, Sydney, NSW, 2052, Australia
[c] LONGI Green Energy Technology Co., Ltd., Xi'an, Shaanxi, 710018, China

A B S T R A C T

Understanding metallic impurities in silicon is essential for the development of silicon-based devices such as solar cells. Transition metals such as iron and chromium have been recognised as harmful impurities in silicon, particularly in p-type silicon. As the photovoltaic industry shifted from boron to gallium doping in p-type silicon, understanding the recombination behaviour of chromium-gallium (CrGa) pairs becomes crucial. This study assesses the recombination parameters of CrGa pairs in silicon using both injection-dependent lifetime spectroscopy (IDLS) and deep-level transient spectroscopy (DLTS). Customised Czochralski (Cz) silicon ingots with known amounts of intentional Cr contamination during the ingot growth process were used, with wafer resistivities varying across the range of 0.2 Ωcm – 8 Ωcm. The presence of Cr in these silicon wafers was first confirmed by monitoring the CrGa pair association and dissociation processes through lifetime-based measurements, which also confirmed the fully paired state of CrGa pairs. The CrGa concentrations in wafers were confirmed by DLTS. Through IDLS and DLTS, the following CrGa defect parameters were extracted: defect energy level $E_t = E_V + 0.47\ eV$, electron capture cross section $\sigma_n = 5.1 \times 10^{-15}\ cm^2$ and hole capture cross section $\sigma_p = 1.1 \times 10^{-15}\ cm^2$.

1. Introduction

The silicon (Si) photovoltaic (PV) industry has rapidly transitioned from using boron (B) to gallium (Ga) as the dopant for p-type silicon wafers, primarily to avoid light-induced degradation caused by boron-oxygen (B-O) defects in silicon [1,2]. In addition, some studies reported a delayed onset and reduced severity of light and elevated temperature induced degradation (LeTID) in Ga-doped wafers compared to the B-doped [3,4]. Transition metals such as iron (Fe) and chromium (Cr) are well known to be common and detrimental impurities in silicon, particularly in p-type silicon [5]. Although the concentrations of Fe and Cr have been quantified previously in multicrystalline and cast-mono silicon materials [6–10], the silicon wafers nowadays from high-quality single-crystalline Czochralski growth (Cz-Si) contain much lower impurity concentrations [11]. The exact concentration of Cr in today's silicon wafers, however, has not been assessed. In the meantime, cell efficiency in industry has also increased drastically in recent years, which demands for increasingly stringent wafer quality and defect control. Therefore, residual defects such as Fe and Cr are crucial to understand and mitigate.

Dissolved Fe and Cr impurities, both in the interstitial form and as metal-acceptor pairs, act as strong recombination centres in the silicon. The recombination parameters related to interstitial Fe and Fe-acceptor pairs in silicon, such as FeB, FeGa, and FeIn pairs, have been well established [12–15]. Studies have also examined the recombination parameters of Cr and CrB pairs in B-doped p-type silicon wafers [16–19]. The formation of CrGa pairs in silicon has been previously reported [20–22]. Similar to CrB, CrGa pairs can be dissociated at elevated temperatures (of around 300 $^\circ C$, as will be shown later in Methodology) but cannot be dissociated by light, unlike FeB or FeGa. This means that during normal solar cell operating conditions under illumination, dissolved Cr impurities in silicon would be in the form of CrGa pairs. It is therefore important to understand the recombination activity of CrGa pairs in silicon to accurately quantify its negative impact. In addition, knowing the recombination parameters of CrGa would enable the use of lifetime-based technique for quantifying Cr concentration in Ga-doped silicon, similar to Ref. [18]. However, a comprehensive analysis of the recombination parameters of CrGa pairs in silicon is still lacking.

In this work, we aim to study the Shockley-Read-Hall (SRH) recombination parameters of CrGa pairs in crystalline silicon. We used specially grown Ga-doped Cz-Si ingots with known amounts of Cr contamination. The presence of Cr in the Ga-doped wafers and the fully paired state of CrGa were first confirmed through measuring the CrGa pairing kinetics. Deep-Level Transient Spectroscopy (DLTS) was then applied to measure the defect energy level (E_t) and hole capture cross section (σ_p), as well as to verify the CrGa defect concentrations. The

* Corresponding author.
E-mail address: anyao.liu@anu.edu.au (A. Liu).

https://doi.org/10.1016/j.solmat.2025.113989
Received 19 July 2025; Received in revised form 18 September 2025; Accepted 29 September 2025
Available online 3 October 2025

CrGa defect concentrations are required for determining the absolute values of the electron and hole capture cross sections (σ_n and σ_p, respectively) from injection-dependent lifetime spectroscopy (IDLS). Room-temperature IDLS was then applied to determine the electron and hole capture cross sections, as well as the defect energy level relative to the mid-bandgap. Here we applied the lifetime linearisation method developed by Murphy *et al.* [23] to further remove potential interference from other defects in the lifetime data. Samples with a range of Ga doping levels $\left(N_A = 1.7\times10^{15}\ cm^{-3} - 9.2\times10^{16}\ cm^{-3}\right)$ and CrGa concentrations $\left(N_t = 8\times10^{11}\ cm^{-3} - 3\times10^{12}\ cm^{-3}\right)$ were analysed to extract a single set of self-consistent SRH parameters that best describe the injection-dependent lifetimes of CrGa pairs in silicon.

2. Methodology

A. Sample preparation

This study used intentionally Cr contaminated Ga-doped Czochralski Si ingots grown at LONGi via the melt recharging method. Two Cr contaminated ingots with two different resistivity ranges were grown. For the high resistivity ingot, Ga doping ranged from 1.7×10^{15} cm^{-3} (seed end) to 2.8×10^{15} cm^{-3} (tail end), which corresponds to resistivities between 8 Ωcm and 5 Ωcm (seed to tail) respectively. The low resistivity ingot had Ga doping concentrations from 1.7×10^{16} cm^{-3} to 9.2×10^{16} cm^{-3}, corresponding to resistivities from 0.9 Ωcm to 0.2 Ωcm (seed to tail) respectively.

The distribution of Cr concentration along the ingots can be estimated from the known amounts of Cr powder added to the Si melt during ingot growth, the known segregation coefficient of Cr in Si, and Scheil's equation [24]. We used the modified Scheil equation to estimate the Cr concentration as a function of solidified fraction in the ingot [25,26].

$$C_S^* = C_0 \times k_{eff} \times (1-f)^{k_{eff}-1} \quad (1)$$

where k_{eff} is the effective segregation coefficient of Cr: 1.1×10^{-5} following Ref [25]; C_0 is the initial solute concentration in the melt before the onset of solidification, which was $7\times10^{16}\ cm^{-3}$ from the known amount of Cr powder added to the Si melt, for both ingots in this study; f is the solidified fraction; and C_S^* is the estimated impurity concentration (Cr in this case). Fig. 1 shows the estimated Cr concentration distribution along the ingot as a function of solidified fraction.

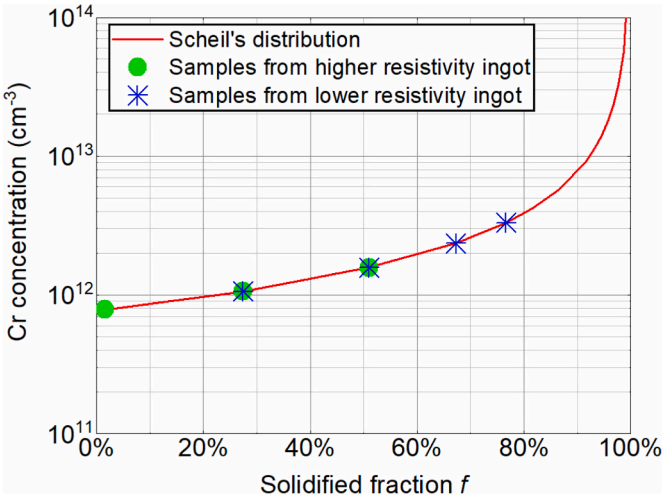

Fig. 1. Cr concentration along an ingot as a function of solidified fraction, estimated from Scheil's distribution and the known amount of Cr addition to the silicon melt. The symbols represent the positions of the two Cr-contaminated ingots where wafers were taken for CrGa analysis in this study. (For interpretation of the references to colour in this figure legend, the reader is referred to the Web version of this article.)

For the high resistivity ingot, which was a shorter ingot, the estimated Cr concentrations varied from 7.8×10^{11} cm^{-3} at the seed end to 1.6×10^{12} cm^{-3} at the tail end; while the low resistivity ingot had Cr concentrations ranging from 7.8×10^{11} cm^{-3} (seed end) to 3.3×10^{12} cm^{-3} (tail end). As will be shown later in Section 3.B., DLTS was applied to measure the CrGa concentrations in some of the higher resistivity samples, and the measured values were found to agree well with those calculated from Scheil's equation.

Prior to growing the two Cr-contaminated ingots, a control ingot without intentional Cr contamination was grown too. The ingot had the same doping levels as the high resistivity ingot described above, that is, resistivities ranged from 8 Ωcm to 5 Ωcm (seed to tail).

The three Cz-Si ingots were sliced into M6-sized wafers with a thickness of 170 − 180 μm, and the solidified fractions of the wafer positions were recorded, accounting for the discarded silicon melt. A total of seven positions were selected from the two Cr-contaminated ingots (three from the high resistivity Cr ingot and four from the low resistivity Cr ingot), with 3–4 wafers from each position to confirm repeatability. Wafers from the exact same positions of the high resistivity control ingot without intentional Cr were included as controls. The M6-sized Cz-Si wafers were then laser-cut into smaller pieces measuring 50 mm by 50 mm. Similar sized boron-doped float-zone (FZ) silicon wafers with a resistivity of 1.3 Ωcm and a thickness of 240 ± 10 μm were included too as additional process controls.

All samples underwent a saw-damage etch of 4 − 5 μm per side using a heated tetramethylammonium hydroxide (TMAH) solution, followed by standard RCA cleaning procedures. Post-cleaning, some samples were passivated with thermal aluminium oxide (Al_2O_3) thin films on both sides using a Beneq TFS 200 series atomic layer deposition (ALD) reactor. These films were prepared by alternating tetramethylammonium (TMA) exposure and H_2O for 300 cycles, resulting in an Al_2O_3 film thickness of approximately 30 nm. To activate the Al_2O_3 passivation, all samples, including control samples, underwent forming gas annealing (FGA) at 425 °C for 30 min. Since the Cr diffusivity in silicon is only moderate [27] and the Al_2O_3 films from thermal ALD were found to be less efficient in gettering in our previous work [28], the impact of Al_2O_3 gettering on the bulk Cr concentration is deemed insignificant.

B. Lifetime measurements and IDLS analysis

Injection-dependent carrier lifetimes of the samples were measured using a photoconductance-based lifetime tester (WCT-120 from Sinton Instruments) at room temperature [29]. The measurement stage temperature was approximately 30 °C. Subsequent injection-dependent lifetime analysis was performed, following the same procedures as in Le *et al.* [12] In short, for the Cr-containing wafers from the high resistivity ingot, the experimentally measured residual lifetime due to CrGa, $\tau_{residual,CrGa}$, was determined from

$$\frac{1}{\tau_{residual,CrGa}} = \frac{1}{\tau_{eff,CrGa}} - \frac{1}{\tau_{eff,control}}, \quad (2)$$

where $\tau_{eff,CrGa}$ represents the measured effective lifetime of the CrGa samples in the fully associated state (detailed below), and $\tau_{eff,control}$ denotes the effective lifetime of the co-processed samples from the control ingot without intentional Cr contamination. The control samples were taken from the same ingot positions, that is, they were of the same resistivities as the Cr samples.

For the Cr-containing wafers from the low resistivity ingot, the residual lifetime due to CrGa was determined by accounting for intrinsic (calculated from Niewelt *et al.* [30]) and surface (experimental) recombination. Surface recombination was estimated from the co-processed wafers from the control ingot without intentional Cr contamination, which had the same ALD Al_2O_3 passivation on both

sides, and a single-sided J_0 in the range of 3–5 fA/cm^2 was extracted (see Fig. S1 in Supplementary Information). This J_0 range corresponds to a surface lifetime of around 10 ms at an injection level of 10^{15} cm^{-3}. Since the effective lifetimes of these low-resistivity Cr-containing wafers were quite low, on the order of a few microseconds to tens of microseconds as will be shown later in Results, surface and intrinsic recombination estimates hardly affect the extraction of $\tau_{residual,CrGa}$ for these samples.

As detailed in our previous publication [12], the lifetime linearisation approach proposed by Murphy *et al.* [23] was then applied to filter out experimental $\tau_{residual,CrGa}$ data that may be affected by the presence of other defects. Representative lifetime curves after linearisation can be found in Supplementary Information (Fig. S2). Only $\tau_{residual,CrGa}$ data showing linearity after linearisation arrangement, with a fitted R^2 value above 0.95, were included for IDLS analysis. Subsequently, SRH model fitting was employed to simultaneously fit the experimental $\tau_{residual,CrGa}$ data to identify the combination of defect parameters that results in the least fitting error.

C. CrGa association kinetics

To confirm the presence of Cr in the Ga-doped samples and to ensure the fully paired state of CrGa for lifetime analysis, CrGa pair dissociation and association experiments were conducted. Equation (3) illustrates the CrGa dissociation and association processes, where dissociation via high temperature was performed at 300 $^{\circ}C$ in this work and association at lower temperatures were carried out at temperatures below 80 $^{\circ}C$, as will be detailed in this section. Cr_i denotes interstitial Cr, and Ga_s denotes substitutional Ga.

$$CrGa \underset{low\ T}{\overset{high\ T}{\rightleftarrows}} Cr_i + Ga_s \tag{3}$$

In this study, dissociation of CrGa pairs was achieved through annealing at 300 $^{\circ}C$ on a hotplate for 5 min, followed by rapid cooling by quenching in water to "freeze" the system in the unpaired state for lifetime measurements. This dissociation temperature (300 °C) was experimentally determined from monitoring sample lifetimes after annealing at a range of temperatures in 150 $^{\circ}C-$ 350 $^{\circ}C$, and little difference in lifetime was observed for temperatures above 275 $^{\circ}C$ (See Fig. S3 in Supplementary Information). Ideally, the binding energy of CrGa pairs would allow one to determine a suitable dissociation temperature. However, there is limited information in the literature about the CrGa binding energy. In addition, CrGa re-pairing would occur during the cool-down process as interstitial Cr is still sufficiently mobile at elevated temperatures. Nevertheless, as the focus of this study is not to achieve 100 % dissociation of CrGa pairs, but to monitor the subsequent CrGa pair association process, an experimentally determined dissociation temperature is sufficient here.

After the dissociation step, CrGa re-pairing kinetics were monitored by measuring the carrier lifetime changes over time at fixed temperatures in 50 $^{\circ}C-$ 80 $^{\circ}C$. The samples were cumulatively annealed at a fixed temperature on a hotplate, and were periodically removed from the hotplate, cooled in air, and measured by a room-temperature lifetime tester (WCT-120). Using the reported binding energy values of CrB (since there is little data on CrGa) [16,31], a vast majority of Cr should be in the paired form of CrGa, rather than interstitial Cr, below 80 $^{\circ}C$ at equilibrium. As will be shown later in Section 3.A., the experimentally measured lifetime changes in this temperature range show decreasing lifetime over time, while a 300 $^{\circ}C$ anneal (meant for pair dissociation) increases the lifetime. The two states can be cycled, confirming the CrGa pair association and dissociation processes.

Control samples without intentional Cr contamination were included in the dissociation and association annealing experiments too, to monitor potential changes in lifetime due to factors other than Cr. The lifetimes of the control samples were found to be stable, ruling out the impact of other recombination sources.

As detailed in a previous work (Equations (3) and (7) in Ref. [19]), the CrGa association kinetics can be characterised by an association time constant, which can be extracted from the experimentally measured lifetime changes over time. Lifetimes at a fixed injection level of $\Delta n = 1 \times 10^{15}$ cm^{-3} were used. From the experimentally extracted association time constants, and knowing the Ga doping levels and association temperatures, the diffusivity values of Cr were estimated (Equation (4) in Ref. [19]) and compared to the literature reported values.

D DLTS measurements

Schottky barrier diodes for DLTS measurements were prepared by mechanical polishing with a Tegramin-25 tool from Struers, enabling an accurate diode area to be determined. The polished samples were cleaned with RCA solutions followed by an HF dip until hydrophobic. Schottky contacts were then formed on the polished side using aluminum and ohmic contacts on the rear were formed using gold. Aluminum was evaporated with a Lesker e-beam evaporator with a 1 mm diameter circular shadow mask; gold was evaporated using a Lesker thermal evaporator on the full rear surface. The quality of the diodes was examined based on current-voltage (IV) and capacitance-voltage (CV) measurements at room temperature. The leakage current at 10 V reverse bias was below 1×10^{-4} A and the fitted doping concentrations aligned with the expected values measured via dark conductance. DLTS measurements were conducted from 100 K to 300 K and the defect densities were analysed based on the amplitudes of the defect peaks and CV results. The defect energy level and capture cross section for holes were extracted from the T^2-corrected Arrhenius plots, following a standard DLTS analysis procedure [32–34]. To ensure the extracted defect parameters are only related to CrGa, the samples experienced a prolonged CrGa association process prior to DLTS measurements.

3. Results and Discussion

A. Confirmation of the presence of Cr

As explained in Section 2.C., to confirm the presence of Cr in the samples, we first analysed the kinetics of lifetime changes upon CrGa association at fixed temperatures in 50 $^{\circ}C-$ 80 °C. Fig. 2 illustrates an example of the changes in effective lifetimes of a sample over time during the association processes of CrGa pairs, occurring at

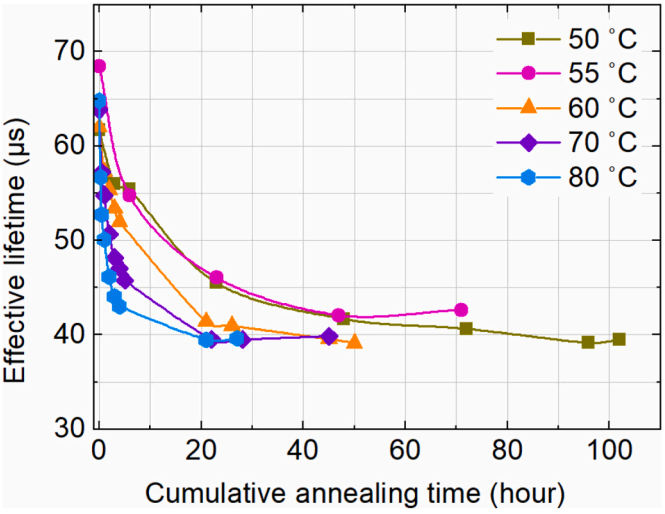

Fig. 2. Evolution of effective carrier lifetimes (at an injection level of 1×10^{15} cm^{-3}) during CrGa pair association processes at 50 $^{\circ}C$ to 80 $^{\circ}C$, for a sample with an $N_A = 2.8 \times 10^{15}$ cm^{-3} and a Cr concentration 1.6×10^{12} cm^{-3} (estimated from Scheil's distribution).

temperatures between 50 °C and 80 °C. Fig. 2 shows that the re-pairing process is faster at higher temperatures, as expected. Additionally, the data show that the lifetime decreases to a similar level during CrGa re-pairing, regardless of the association temperature, confirming the fully paired state of CrGa. These steady state lifetimes are therefore suitable for subsequent IDLS analysis to extract the defect parameters of CrGa in Si.

Next, we compared the diffusivity values extracted from our experimental CrGa association time constants with those reported in the literature from various studies, as illustrated in Fig. 3. The CrGa association time constants were extracted from samples with a range of resistivities (0.2 Ωcm – 8 Ωcm). Fig. 3 clearly shows that the Cr diffusivities obtained from our CrGa association processes at 50 °C to 80 °C align well with the Cr diffusivity values reported in the literature. This agreement confirms the presence of Cr in our test samples.

B. Deep Level Transient Spectroscopy (DLTS)

DLTS was used to measure the CrGa defect concentration (N_t), defect energy level (E_t), and hole capture cross section (σ_p). Because of the DLTS detection limit, only samples from the high resistivity ingots (with resistivities ranging from 5 Ωcm to 8 Ωcm) could be measured by DLTS. The DLTS spectra and the associated T^2-corrected Arrhenius plots are shown in Fig. 4. In Fig. 4(a), both DLTS spectra demonstrate a peak at about 260 K, which is shown to agree well with the identification of CrGa by applying the E_t and σ_p parameters reported in Graff [5]. The CrGa concentrations (N_t) measured by DLTS were 8.4×10^{11} cm^{-3} for the 8 Ωcm and 1.1×10^{12} cm^{-3} for the 5 Ωcm samples, respectively. These agree well with the estimated Cr (i.e. CrGa in the fully paired state) concentrations of 7.8×10^{11} cm^{-3} and 1.6×10^{12} cm^{-3}, respectively, from the known Cr contamination in the ingot and Scheil's distribution, as described previously in Methodology (Fig. 1). Therefore, the estimated Cr concentrations from Scheil's distribution were used as input N_t values in the subsequent IDLS analysis to extract the hole and electron capture cross sections (σ_p and σ_n) in the following Section C.

A linear fit to both DLTS Arrhenius plots in Fig. 4(b) results in a CrGa defect energy level of $E_t = E_v + 0.47$ eV and a hole capture cross section of $\sigma_p = 1.1\times 10^{-15}$ cm^2. As shown in Fig. 4(b), the data also agree well with the literature reported values listed in Graff [5].

C Injection Dependent Lifetime Spectroscopy (IDLS) Analysis

The injection-dependent lifetime curves related to CrGa, expressed as $\tau_{residual,CrGa}$ above, from the full set of samples with varying doping and defect concentrations, were then simultaneously fit by SRH statistics in order to extract a single set of defect parameters (E_t, σ_p, σ_n) that results in the best fitting. To visualise the fitting results, Fig. 5 plots the fitting errors (see Ref. [12] for detailed definition) as a function of the input defect parameters.

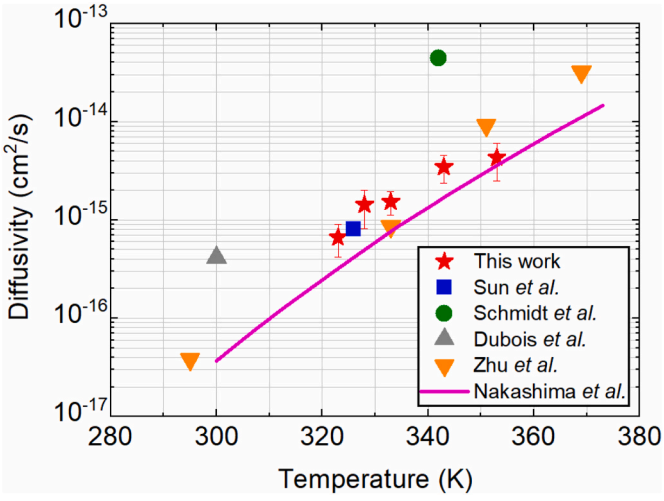

Fig. 3. A comparison of the Cr diffusivity values extracted from the CrGa pair association experiments (50 °C −80 °C) in this work, with the literature reported values [17–19,27,35].

Since the CrGa defect energy level can be unambiguously determined by DLTS, and this E_t value is shown to agree very well with the literature (see Table 1), we first fixed the defect energy level at $E_t = E_v + 0.47$eV and varied the electron and hole capture cross section values. As shown in Fig. 5 (a), the fitting is sensitive to the input σ_n and σ_p values, allowing the best-fit values to be extracted (summarised in Table 1).

Subsequently, fixing $\sigma_n = 5.1\times 10^{-15}$ cm^2, Fig. 5(b) explored the dependence of the fitting error on the input σ_p and E_t values. Fig. 5 (b) allowed us to narrow down the σ_p value to 1.2×10^{-15} cm^2. This is in excellent agreement with the DLTS extracted $\sigma_p = 1.1\times 10^{-15}$ cm^2. However, in Fig. 5 (b) we observed a wide range of E_t values (from E_v + 0.3 eV to E_v + 0.75 eV) that can produce a minimum fitting error. This clearly demonstrates the insensitivity of the IDLS method to identify the defect energy level here. Therefore, the DLTS measured defect energy level is reported in Table 1.

Fig. 6 presents the experimental and simulated lifetime curves due to CrGa pairs. The simulated SRH lifetimes due to CrGa were calculated using the defect parameters in this study, as summarised in Table 1. As shown in Fig. 6, the experimental and simulated lifetimes show reasonable agreement for the whole set of the samples. It is noted that the discrepancy seems to become larger for some of the more heavily doped samples from the near tail part of the low resistivity ingot. This may be related to the larger uncertainty in estimating CrGa concentration from Scheil's distribution as the solidified fraction increases (Fig. 1). However, this is speculative and needs further investigation.

D.Simulated SRH lifetimes and comparison to the literature

Fig. 7 compares the simulated SRH lifetimes for CrGa, using the defect parameters from this study (Table 1) and from Beljakowa *et al.*, [20] as well as the SRH lifetimes for CrB using the defect parameters from Sun *et al.* [19] Here we assumed a defect concentration of 10^{10} cm^{-3}, which is lower than the intentional contamination levels used in this work but is possible in industrial Cz-Si wafers used for solar cells, especially wafers from the tail end of the Cz-Si ingots [11,36].

Comparing the CrGa lifetimes in Fig. 7, it can be clearly seen that the parameters from Beljakowa *et al.* [20] produce lifetimes that are lower than ours by more than one order of magnitude, although the shape of the curves is similar. This can be explained by the same defect energy level, similar capture cross section ratios but larger values of electron and hole capture cross sections reported in Beljakowa *et al.*, [20] as shown in Table 1.

However, Beljakowa *et al.*'s extraction of CrGa capture cross sections were very likely affected by the following factors. Firstly, FeGa was clearly detected in their Cr-implanted and Cr-diffused samples. FeGa has capture cross sections that are on the order of 10^{-14} cm^2 [12] and is more recombination active than CrGa shown in this study. Moreover, the FeGa concentrations detected in their Cr-implanted samples were significant, ranging from 15 % to 50 % of the measured CrGa concentrations. Therefore, the presence of FeGa could have obscured the measured effective lifetimes of their CrGa samples, and the impact of FeGa was not considered in Beljakowa *et al.*'s analysis. In this work, we attempted to assess the concentration of unintentional Fe_i in the samples by measuring the lifetimes before and after strong illumination, a well-known method for measuring Fe_i in p-type silicon [12,37,38]. However, little change in lifetimes could be observed before and after illumination, indicating that Fe or FeGa has a negligible effect on the measured effective lifetimes in this work. Representative lifetime curves before and after illumination are shown in Fig. S4 in Supplementary

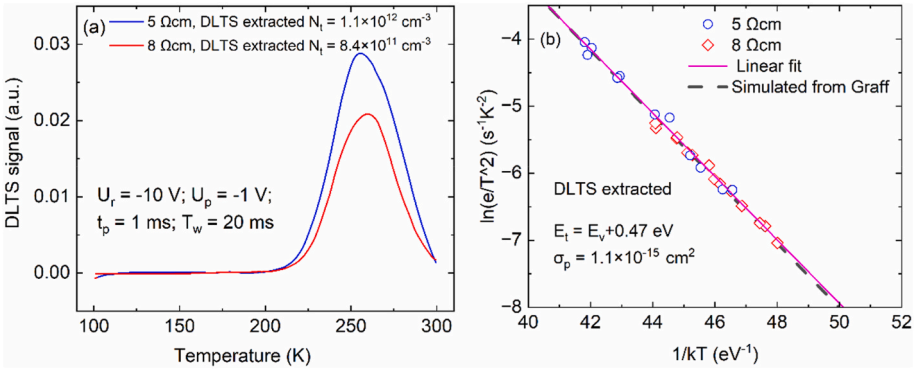

Fig. 4. (a) DLTS spectra measured on Cr-contaminated Ga-doped silicon wafers of 5 Ωcm and 8 Ωcm, in the CrGa fully paired state. (b) Arrhenius plots of these two samples (symbols), and a linear fit to both data (solid line). The dashed line is simulated based on the reported E_t and σ_p values from Graff [5]. The DLTS measurement conditions are listed in (a). (For interpretation of the references to colour in this figure legend, the reader is referred to the Web version of this article.)

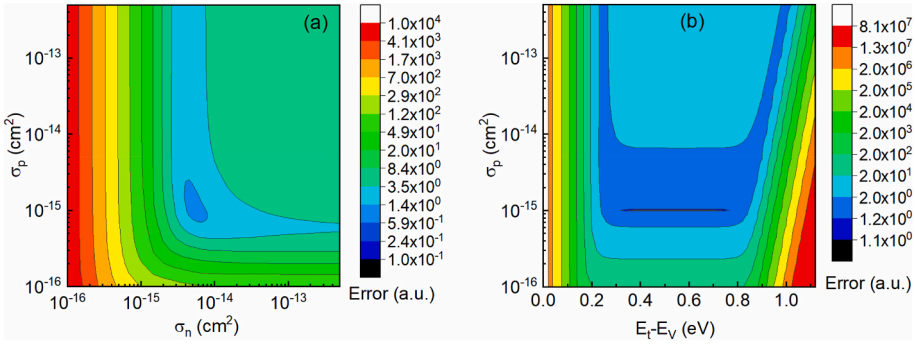

Fig. 5. IDLS analysis to visualise the combination of defect parameters that results in the least error (i.e. best fit) to the experimentally measured injection-dependent $\tau_{residual,CrGa}$ data: (a) varying σ_n and σ_p while fixing $E_t = E_v + 0.47$ eV, and (b) varying E_t and σ_p while fixing$\sigma_n = 5.1 \times 10^{-15}$ cm^2. The colour bars indicate the average errors in simultaneously fitting the experimental data by SRH modelling based on the given combination of defect parameters. The fitting was applied to the full set of the samples with varying resistivities and defect concentrations. (For interpretation of the references to colour in this figure legend, the reader is referred to the Web version of this article.)

Table 1
A summary of CrGa recombination parameters, from this study and the literature.

Defect Energy Level $E_t - E_v$ (eV)	Electron capture cross section σ_n (cm^2)	Hole capture cross section σ_p (cm^2)	Capture cross section ratio $k = \frac{\sigma_n}{\sigma_p}$	Method	Ref
0.47	5.1×10^{-15}	1.1×10^{-15}	4.6	IDLS, DLTS	This work
0.47	7.1×10^{-14}	2.1×10^{-14}	3.4	IDLS, DLTS	Beljakowa *et al.* [20]
0.48	–	1.5×10^{-15}	–	DLTS	Graff [5]

Information.

Secondly, the samples for lifetime measurements in Beljakowa *et al.* were not surface passivated, demonstrating very low lifetimes below a few microseconds. As shown in Fig. 6, with good surface passivation, the CrGa lifetimes can reach tens of microseconds. The dominance of surface-limited lifetime in their samples would lead to inaccurate analysis of bulk defects. Lastly, their lifetime analysis was restricted to low-injection conditions rather than fitting the entire injection range. Therefore, by carefully excluding the impact of other defects through co-processed control samples and lifetime linearisation, we are much more confident in the CrGa capture cross sections presented in this study.

Comparing CrGa (from this study's reported parameters) and CrB

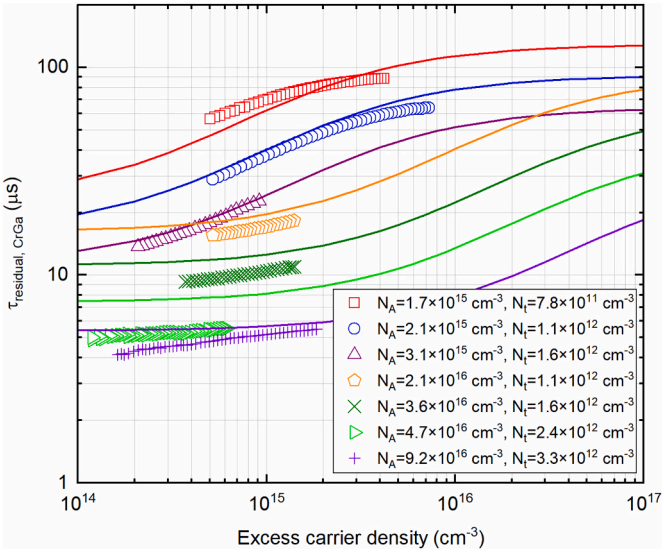

Fig. 6. Injection-dependent lifetime curves of the Cr-contaminated samples of varying N_A and N_t: the symbols are experimentally measured CrGa lifetimes ($\tau_{residual,CrGa}$), and the solid lines are the simulated SRH lifetimes due to CrGa based on the defect parameters extracted from this study.

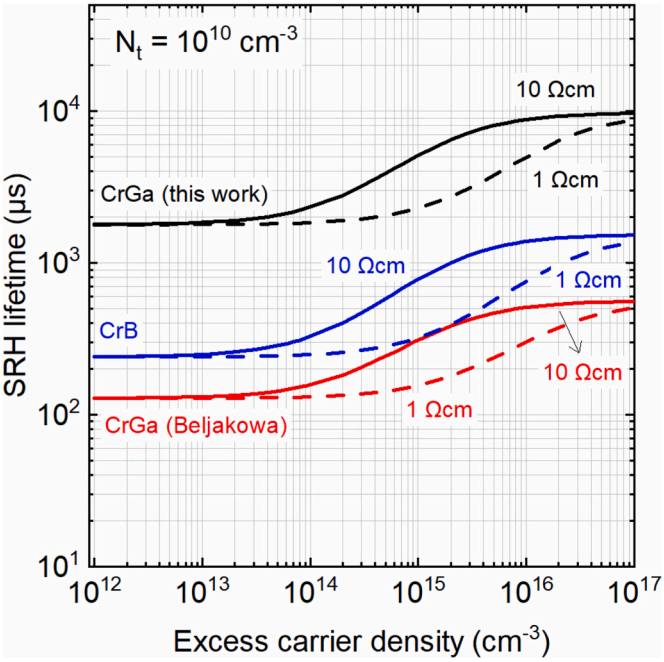

Fig. 7. Simulated injection-dependent SRH lifetime based on the defect parameters of CrGa from this work and from Beljakowa *et al.* [20] and CrB from Sun *et al.* [19], for a defect concentrations of $N_t = 1 \times 10^{10}$ cm^{-3} and two different resistivities of 1 Ωcm and 10 Ωcm.

lifetimes, it is interesting to note that CrGa pairs are less recombination active than CrB pairs, which can be seen as an additional advantage of Ga doping over B doping in the presence of residual Cr contamination. The simulation in Fig. 7 also shows that increasing wafer resistivity from 1 Ωcm to 10 Ωcm slightly increases the SRH lifetimes in the mid-injection range.

4. Conclusion

This study investigated the recombination parameters of CrGa pairs in p-type silicon. Intentionally chromium-contaminated, gallium-doped silicon wafers with resistivities ranging from 8 Ωcm to 0.2 Ωcm were used. The presence of Cr in these specially grown samples was first confirmed by analysing CrGa association kinetics, which also confirmed the fully paired state of CrGa. The concentration of CrGa was confirmed by deep-level transient spectroscopy (DLTS). DLTS and injection-dependent lifetime spectroscopy (IDLS) were then applied to extract the CrGa defect energy level, and electron and hole capture cross sections. The defect energy level is found to agree very well with the literature. DLTS and IDLS produced a consistent hole capture cross section. A new set of electron and hole capture cross sections is reported. By carefully eliminating the potential impact of other defects through co-processed control samples and lifetime linearisation, we provide confidence to our reported CrGa capture cross sections compared to those reported by Beljakowa *et al.* [20].

CRediT authorship contribution statement

Sanjida Sabah: Writing – original draft, Visualization, Investigation, Formal analysis, Data curation. **Tien T. Le:** Writing – review & editing, Visualization, Software, Methodology, Formal analysis, Data curation. **Zhuangyi Zhou:** Writing – review & editing, Visualization, Methodology, Investigation, Formal analysis. **Chang Sun:** Writing – review & editing, Resources. **Yichun Wang:** Resources. **Nannan Fu:** Resources. **Fiacre Rougieux:** Writing – review & editing, Resources. **Daniel Macdonald:** Writing – review & editing, Supervision, Resources, Project administration, Funding acquisition. **AnYao Liu:** Writing – review & editing, Writing – original draft, Visualization, Supervision, Software, Project administration, Methodology, Formal analysis, Conceptualization.

Declaration of competing interest

The authors declare the following financial interests/personal relationships which may be considered as potential competing interests: Daniel Macdonald reports financial support was provided by Australian Centre for Advanced Photovoltaics. AnYao Liu reports financial support was provided by Australian Centre for Advanced Photovoltaics. Chang Sun reports a relationship with LONGi Green Energy Technology Co Ltd that includes: employment. Yichun Wang reports a relationship with LONGi Green Energy Technology Co Ltd that includes: employment. Nannan Fu reports a relationship with LONGi Green Energy Technology Co Ltd that includes: employment. If there are other authors, they declare that they have no known competing financial interests or personal relationships that could have appeared to influence the work reported in this paper.

Acknowledgement

This work was supported by the Australian Renewable Energy Agency (ARENA) through the Australian Centre for Advanced Photovoltaics (ACAP).

Appendix A. Supplementary data

Supplementary data to this article can be found online at https://doi.org/10.1016/j.solmat.2025.113989.

Data availability

Data will be made available on request.

References

[1] A. Metz, T. Abe, R. Hezel, Gallium-doped Czochralski grown silicon: a novel promising material for the PV-industry, Proc. 16th EU-PVSEC, Glasgow (2000) 1189.
[2] A.R. Meyer, et al., Spectroscopic investigation of shallow hole traps in Ga-and B-doped Czochralski silicon: insight into light-induced degradation, ACS Appl. Energy Mater. 5 (11) (2022).
[3] N.E. Grant, et al., Lifetime instabilities in gallium doped monocrystalline PERC silicon solar cells, Sol. Energy Mater. Sol. Cell. 206 (2020) 110299.
[4] T. Niewelt, et al., Stability of industrial gallium-doped Czochralski silicon PERC cells and wafers, Sol. Energy Mater. Sol. Cell. 266 (2024) 112645.
[5] K. Graff, Metal Impurities in silicon-device Fabrication, vol. 24, Springer Science & Business Media, 2013.
[6] A.A. Istratov, et al., Metal content of multicrystalline silicon for solar cells and its impact on minority carrier diffusion length, J. Appl. Phys. 94 (10) (2003) 6552–6559.
[7] A. Liu, et al., Gettering of transition metals in high-performance multicrystalline silicon by silicon nitride films and phosphorus diffusion, J. Appl. Phys. 125 (4) (2019).
[8] D. Macdonald, et al., Transition-metal profiles in a multicrystalline silicon ingot, J. Appl. Phys. 97 (3) (2005).
[9] G. Stokkan, et al., Impurity control in high performance multicrystalline silicon, Phys. Status Solidi 214 (7) (2017) 1700319.
[10] C. Sun, et al., Transition metals in a cast-monocrystalline silicon ingot studied by silicon nitride gettering, Phys. Status Solidi Rapid Res. Lett. 13 (12) (2019) 1900456.
[11] R. Basnet, et al., Investigating wafer quality in industrial Czochralski-Grown gallium-doped p-Type silicon ingots with melt recharging, Sol. RRL 7 (15) (2023).
[12] T.T. Le, et al., Reassessing iron–gallium recombination activity in silicon, J. Appl. Phys. 135 (13) (2024).
[13] J. Schmidt, D. Macdonald, Recombination activity of iron-gallium and iron-indium pairs in silicon, J. Appl. Phys. 97 (11) (2005).
[14] A. Istratov, H. Hieslmair, E. Weber, Iron and its complexes in silicon, Appl. Phys. A 69 (1) (1999) 13–44.
[15] D. MacDonald, et al., Doping dependence of the carrier lifetime crossover point upon dissociation of iron-boron pairs in crystalline silicon, Appl. Phys. Lett. 89 (14) (2006).

[16] H. Conzelmann, K. Graff, E. Weber, Chromium and chromium-boron pairs in silicon, Appl. Phys. A 30 (1983) 169–175.
[17] S. Dubois, O. Palais, P. Ribeyron, Determination at 300K of the hole capture cross section of chromium-boron pairs in p-type silicon, Appl. Phys. Lett. 89 (23) (2006).
[18] J. Schmidt, et al., Recombination activity of interstitial chromium and chromium-boron pairs in silicon, J. Appl. Phys. 102 (12) (2007).
[19] C. Sun, F.E. Rougieux, D. Macdonald, Reassessment of the recombination parameters of chromium in n-and p-type crystalline silicon and chromium-boron pairs in p-type crystalline silicon, J. Appl. Phys. 115 (21) (2014).
[20] S. Beljakowa, Fe-und Cr-korrelierte Defekte in Einkristallinem Si: Ga Und Elektrische Eigenschaften Von Multikristallinem Si, Friedrich-Alexander-Universitaet Erlangen-Nuernberg, 2005 (Germany). PhD thesis.
[21] H. Feichtinger, J. Oswald, R. Czaputa, P. Vogl, K. Wunstel, in: L.C. Kimerling, J. M. Parsey (Eds.), 13th Int Conf. On Defects in Semiconductors (Coronado 1984), Metallurgical Soc. AIME, Warrendale, PA, 1984, p. 855.
[22] H. Lemke, Ionenpaare zwischen Chrom und flachen Akzeptoren in Silizium, Phys. Status Solidi 75 (1) (1983) K49–K51.
[23] J.D. Murphy, et al., Parameterisation of injection-dependent lifetime measurements in semiconductors in terms of shockley-read-hall statistics: an application to oxide precipitates in silicon, J. Appl. Phys. 111 (11) (2012).
[24] E. Scheil, Bemerkungen zur schichtkristallbildung, Int. J. Mater. Res. 34 (3) (1942) 70–72.
[25] R.A. Brown, Modelling of directional solidification: from Scheil to detailed numerical simulation, J. Cryst. Growth 109 (1–4) (1991) 50–65.
[26] R. Hopkins, et al., Crystal growth considerations in the use of “solar grade” silicon, J. Cryst. Growth 42 (1977) 493–498.
[27] H. Nakashima, et al., Diffusion and electrical properties of 3d transition-metal impurity series in silicon, in: Materials Science Forum, 1993.
[28] T.T. Le, et al., Gettering of iron by aluminum oxide thin films on silicon wafers: kinetics and mechanisms, J. Appl. Phys. 135 (6) (2024).
[29] R.A. Sinton, A. Cuevas, Contactless determination of current–voltage characteristics and minority-carrier lifetimes in semiconductors from quasi-steady-state photoconductance data, Appl. Phys. Lett. 69 (17) (1996) 2510–2512.
[30] T. Niewelt, et al., Reassessment of the intrinsic bulk recombination in crystalline silicon, Sol. Energy Mater. Sol. Cell. 235 (2022) 111467.
[31] H. Habenicht, M.C. Schubert, W. Warta, Imaging of chromium point defects in p-type silicon, J. Appl. Phys. 108 (3) (2010).
[32] D. Lang, Deep-level transient spectroscopy: a new method to characterize traps in semiconductors, J. Appl. Phys. 45 (7) (1974) 3023–3032.
[33] A. Peaker, M. Brozel, Electrical techniques for the measurement of deep states, III-Vs Rev. 12 (1) (1999) 44–51.
[34] Z. Zhou, et al., Electronic properties of the boron–oxygen defect precursor of the light-induced degradation in silicon, IEEE J. Photovoltaics 12 (5) (2022) 1135–1141.
[35] J. Zhu, et al., Interstitial chromium behaviour in silicon during rapid thermal annealing, Appl. Surf. Sci. 36 (1–4) (1989) 413–420.
[36] T. Le, et al., Industrial Czochralski n-type silicon wafers: gettering effectiveness and possible bulk limiting defects, Sol. RRL 8 (6) (2024).
[37] D. Macdonald, L.J. Geerligs, A. Azzizi, Iron detection in crystalline silicon by carrier lifetime measurements for arbitrary injection and doping, J. Appl. Phys. 95 (3) (2004) 1021–1028.
[38] G. Zoth, W. Bergholz, A fast, preparation-free method to detect iron in silicon, J. Appl. Phys. 67 (11) (1990) 6764–6771.